Acta Crystallographica Section F
Structural Biology and Crystallization Communications
ISSN 1744-3091

Structural analysis of *Pneumocystis carinii* dihydrofolate reductase complexed with NADPH and 2,4-diamino-6-[2-(5-carboxypent-1-yn-1-yl)-5-methoxybenzyl]-5-methylpyrido[2,3-*d*]pyrimidine

Vivian Cody,[a,b]* Jim Pace[a] and Elizabeth Stewart[a]

[a]Structural Biology Department, Hauptman–Woodward Medical Research Institute, 700 Ellicott Street, Buffalo, NY 14203, USA, and [b]Structural Biology Department, School of Medicine and Biological Sciences, State University of New York at Buffalo, Buffalo, NY 14260, USA

Correspondence e-mail: cody@hwi.buffalo.edu

Received 8 February 2012
Accepted 27 February 2012

PDB Reference: pcDHFR–NADPH–PY1014 complex, 3td8.

Structural data are reported for 2,4-diamino-6-[2-(5-carboxypent-1-yn-1-yl)-5-methoxybenzyl]-5-methylpyrido[2,3-*d*]pyrimidine (PY1014) complexed with *Pneumocystis carinii* dihydrofolate reductase (pcDHFR) refined to 1.8 Å resolution. These data reveal that the carboxylate of the ω-carboxyalkynyl side chain of PY1014, the most pcDHFR-selective analog in this series, forms ionic interactions with the conserved Arg75 in the substrate-binding pocket of pcDHFR. The reversal of the 2′,5′-substitution pattern of this analog compared with the highly selective diaminopyrimidine analog PY1011 (*i.e.* the 5′-pentynylcarboxy-5′-methoxy pattern of PY1014 *versus* the 3′,4′-dimethoxy-5′-pentynylcarboxy pattern of PY1011) is necessary to achieve optimal interaction with Arg75 as observed in other structures. The larger diaminopyrido[2,3-*d*]-pyrimidine ring of PY1014 places the 5′-methoxy group closer to Leu25 and Ser64 than does the diaminopyrimidine ring of PY1011. The 5′-methoxy O atom forms a hydrogen bond to the amide of Leu25 (O$\cdots$N, 2.7 Å) and the 5′-methoxy methyl group makes a hydrophobic contact of 3.1 Å with C^{β} of Ser64. Although the IC_{50} values of PY1014 and PY1011 are similar, inhibition data show that the selectivity of PY1011 for pcDHFR is significantly greater. The greater selectivity for pcDHFR compared with mammalian DHFR of these inhibitors is also influenced by the enhanced hydrophobic interactions of the side-chain methylene atoms with Phe69 of pcDHFR compared with Asn64 of mammalian DHFR.

1. Introduction

The antimicrobial agent trimethoprim (TMP; Fig. 1) is still extensively used for prophylaxis and/or therapy of opportunistic infections by *Pneumocystis* pathogens, which are still a leading cause of mortality and morbidity among patients with AIDS or other immunosuppressive conditions (Thomas & Limper, 2004). The primary treatment for *Pneumocystis* pneumonia (PcP) combines a sulfonamide drug with TMP, which targets the folate pathway, although its use in combination therapy with a sulfonamide that targets the dihydropteroate pathway is not always successful (Rosowsky *et al.*, 2003). TMP has limited efficacy in PcP patients and can result in drug resistance (Nahimana *et al.*, 2004). Therefore, there is still a need to develop more effective treatments.

As part of a larger program to design lipophilic DHFR inhibitors that would contain structural features of both piritrexim (PTX) and TMP (Fig. 1), Rosowsky and coworkers synthesized a number of compounds that incorporated the 2′,5′-dimethoxybenzyl substitution pattern of PTX and the diaminopyrimidine-5-(3′,4′,5′-trimethoxybenzyl) pattern of TMP (Chan *et al.*, 2005; Forsch *et al.*, 2004; Rosowsky *et al.*, 2004). To further define inhibitor classes that combined the high potency of PTX with the high antiparasitic *versus* mammalian selectivity of TMP, a series of 2,4-diamino-6-(2′,5′-disubstituted-benzyl)pyrido[2,3-*d*]pyrimidines with *O*-(ω-carboxyl-alkyl) or ω-carboxy-1-alkynyl groups on the benzyl moiety were designed and tested as inhibitors of *P. carinii* dihydrofolate reductase (pcDHFR; Chan *et al.*, 2005).

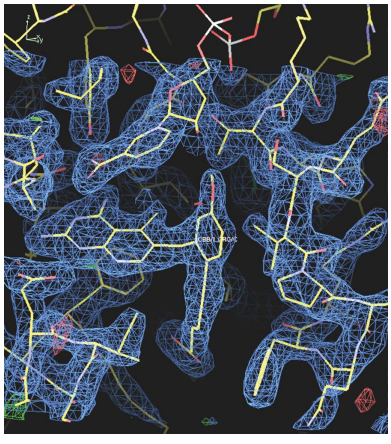

Structure–activity correlations for the series of diaminopyrimidines that have the TMP template revealed that the optimal length of the ω-carboxyalkoxy side chain was the carboxy-1-pentynylbenzyl side chain of PY1011 (Fig. 1), which had a selectivity ratio of 5000 for rat DHFR/pcDHFR IC_{50} (Table 1). However, the analog with the greatest potency was PY957, which has a carboxybutyloxybenzyl side chain (Fig. 1) and a selectivity ratio of 80 (Rosowsky *et al.*, 2004). The sequence of rat liver DHFR has 89% identity and 96% similarity to that of human DHFR and none of the differences involve active-site residues.

Structural data for PY1011, PY996 and PY957 revealed that the inhibitor carboxylate formed a strong salt bridge with the conserved Arg75 in the pcDHFR active site, similar to that observed for the folate substrate or methotrexate inhibitor complexes (Cody *et al.*, 1999, 2006; Cody & Pace, 2011). The orienting effect of the partially rigid 1-pentynyl moiety in PY1011 results in the placement of the methylene C atoms of the side chain closer to Phe69 than those in PY957. These differences help to explain the enhanced selectivity of PY1011 for pcDHFR compared with PY957 or PY996 (Cody *et al.*, 2006; Cody & Pace, 2011). Furthermore, the addition of the 3′,4′-dimethoxy substitution pattern in PY1011 is an important contributor to its enhanced potency towards pcDHFR compared with PY957, as the 3′,4′-dimethoxy groups make additional hydrophobic contacts with the surrounding residues. The greater selectivity of these inhibitors for pcDHFR is also enhanced by the hydrophobic contacts of Phe69 with the methylene C atoms of the side chain, whereas in mammalian DHFR this position is occupied by Asn64, reducing the hydrophobic binding interactions with the side-chain methylene C atoms of the inhibitors.

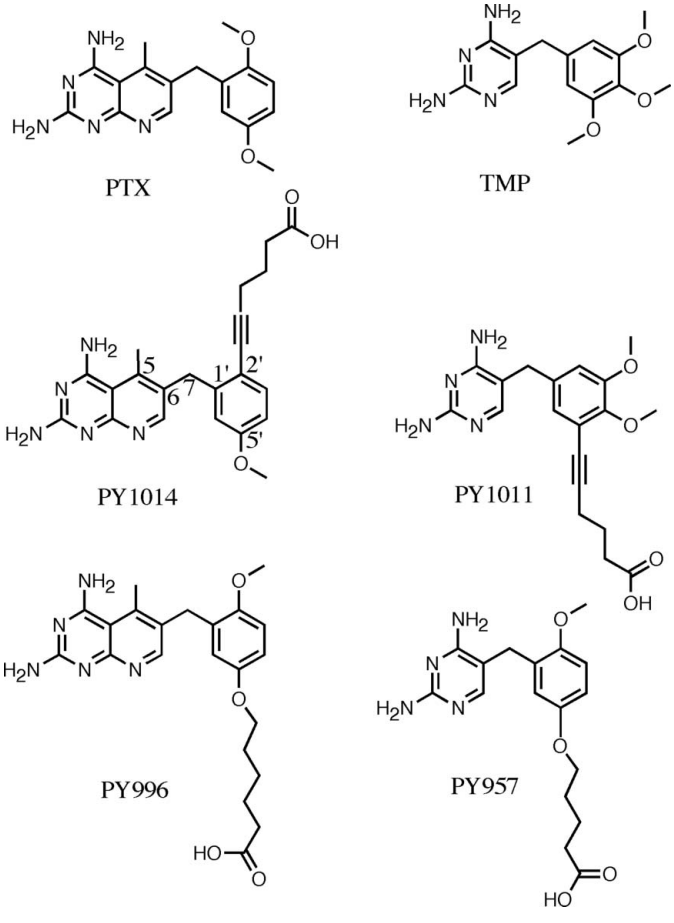

Figure 1
Schematic representation of the antifolates under study.

Table 1
DHFR enzyme-inhibition and selectivity data for the inhibitors shown in Fig. 1.

The values are taken from previously published data (Chan *et al.*, 2005).

Analog	IC_{50} pcDHFR (n*M*)	IC_{50} rlDHFR (n*M*)	rlDHFR/ pcDHFR	C5–C6–C7–C1′ (°)	C6–C7–C1–C2′ (°)
PTX	13	3.3	0.26	123.5	108.8
PY1014	1.2	24	20	121.9	106.7
PY996	1.3	2.0	1.5	−58.8	−87.1
TMP	1000	189000	14.5	201.0†	66.1
PY1011	1.0	5000	5000	177.2†	−105.9
PY957	0.049	3.9	80	179.1†	−88.9

† The torsion angles for the pyrimidine inhibitors are C4–C5–C7–C1′ and C5–C7–C1′–C2′.

To understand the effect of the pyrido[2,3-*d*]pyrimidine ring *versus* the pyrimidine ring of the carboxy-1-alkynyl or carboxy-1-alkoxy series on potency and selectivity against pcDHFR, a series of pyrido[2,3-*d*]pyrimidine analogs with similar side chains including ester derivatives were studied (Chan *et al.*, 2005; Rosowsky *et al.*, 2004; Cody & Pace, 2011). The potency of this series for pcDHFR was uniformly reduced, with the most selective analog being PY1014 (Fig. 1), which has an IC_{50} for pcDHFR of 1.2 n*M* (Table 1). This inhibitor is similar to its pyrimidine analog PY1011 (Fig. 1), which has an IC_{50} of 1.0 n*M*. However, PY1014 is significantly less selective and has a rat liver DHFR (rlDHFR)/pcDHFR selectivity ratio of 20 compared with 5000 for PY1011 (Chan *et al.*, 2005). The potency of PY1014 is also similar to that of the pyrido[2,3-*d*]pyrimidine analog PY996 (IC_{50} 1.3 n*M*), which has a similar substitution pattern to the pyrimidine analog PY957 (IC_{50} 0.05 n*M*; Fig. 1); however, the selectivity ratio between rlDHFR and pcDHFR for PY996 is only 1.5 compared with 80 for PY957 (Table 1; Chan *et al.*, 2005; Cody *et al.*, 2006). In order to validate the binding mode of PY1014, we report structural data for its ternary complex with NADPH and pcDHFR.

2. Methods

2.1. Crystallization and X-ray data collection

Recombinant pcDHFR was cloned, expressed and purified as described previously (Cody *et al.*, 2009). The protein was washed in a Centricon-10 three times with 10 m*M* MES buffer pH 6.0, 100 m*M* KCl and concentrated to 12.5 mg ml^{-1}. The protein was incubated with a tenfold excess of NADPH and 10 m*M* PY1014 prior to crystallization using the hanging-drop vapor-diffusion method at 277 K. The protein drops for pcDHFR complexes consisted of a 1:1 mixture of protein and 33–36% PEG 2K, 46–52 m*M* MES pH 6 with 100 m*M* KCl. Cryogenic solutions for the pcDHFR crystals were prepared using mother liquor with a 16–24% gradient of ethylene glycol. Crystals of pcDHFR complexes grew as thin plates that tended to have a high mosaicity and to give rise to anisotropic distributions in their diffraction limits.

Data for the pcDHFR–inhibitor complex were collected to 1.8 Å resolution on beamline 9-2 at the Stanford Synchrotron Radiation Lightsource (SSRL) using the remote-access protocol (McPhillips *et al.*, 2002; Cohen *et al.*, 2002; González *et al.*, 2008). The data were processed with *HKL*-2000 using *DENZO* (Otwinowski & Minor, 1997) and were scaled with *SCALA* (Evans, 2006). The unit-cell parameters and diffraction statistics are listed in Table 2.

2.2. Structure determination and refinement

The structure of the ternary complex of pcDHFR with PY1014 and NADPH was solved by the molecular-replacement method with *MOLREP* (Vagin & Teplyakov, 2010) as implemented in the *CCP*4 suite of programs (Winn *et al.*, 2011) using the coordinates of pcDHFR (PDB entry 3cd2; Cody *et al.*, 1999). Inspection of the resulting electron-density maps was made using the program *Coot* (Emsley *et al.*, 2010) running on an iMac OS X workstation and revealed density for a ternary complex. To monitor the refinement, a random subset (5%) of all reflections was set aside for the calculation of R_{free}. The models for PY1014 and the cofactor were prepared using the *PRODRG*2 server website (http://davapc1.bioch.dundee.ac.uk/programs/prodrg; Schüttelkopf & van Aalten, 2004). Refinement was carried out using the program *REFMAC*5 (Murshudov *et al.*, 2011) as implemented in the *CCP*4 suite of programs (Winn *et al.*, 2011). Between least-squares minimizations, the structure was manually adjusted to fit the observed electron density. The Ramachandran conformational parameters generated by *RAMPAGE* (Lovell *et al.*, 2002) for the final models from the last cycle of refinement are listed in Table 2. Coordinates for this structure have been deposited in the Protein Data Bank (PDB entry 3td8). Superimpositions were computed with the *SSM* function (Krissinel & Henrick, 2004) in *Coot* (Emsley *et al.*, 2010) using the same reference structure. Figures were prepared using the modeling program *PyMOL* (DeLano, 2002).

Table 2
Crystal properties and data-collection and refinement statistics.

Values in parentheses are for the highest resolution shell.

Crystal properties	
Space group	$P2_1$
Unit-cell parameters	
a (Å)	36.12
b (Å)	42.63
c (Å)	59.89
β (°)	95.2
Data collection	
Beamline	SSRL 9-2
Resolution range (Å)	59.7–1.80 (1.90–1.80)
Wavelength (Å)	0.975
R_{merge}	0.07 (0.62)
Completeness (%)	95.9 (76.8)
Observed reflections	55637 (4320)
Unique reflections	16268 (1843)
$\langle I/\sigma(I)\rangle$	10.7 (1.4)
Multiplicity	3.4 (2.3)
Refinement	
Resolution range (Å)	35.9–1.80
Reflections used	15433
R factor (%)	19.7
R_{free} (%)	25.9
No. of protein/ligand atoms	1780
No. of water molecules	44
B factor (protein average) (Å^2)	37.9
Error in Luzzati plot	0.24
R.m.s. deviation from ideal	
Bond lengths (Å)	0.024
Bond angles (°)	2.35
Ramachandran plot, residues in (%)	
Most favored region	93.1
Allowed region	5.9
Disallowed	1.0
Residues missing density†	1–4, 84–92
PDB code	3td8

† Residues without interpretable density (not refined).

3. Results

Inspection of the electron-density maps for pcDHFR complexed with PY1014 (Fig. 2) revealed a ternary complex with NADPH. The lack of clearly interpretable electron density for loop 83–92 in this pcDHFR complex indicates that this region is highly mobile and represents alternate conformational states compared with the structures previously reported in other pcDHFR complexes (Cody *et al.*, 1999; Cody & Schwalbe, 2006; Cody & Pace, 2011). Similarly, there was poor electron density for the first four N-terminal residues. These residues were not included in the refinement. As illustrated in Fig. 3, there are several loop regions on the surface of the protein that have higher thermal motion, as reflected in their increased B values, which range between 50 and 70 Å^2 compared with 20–30 Å^2 for the more stable regions.

As previously described (Cody *et al.*, 2005, 2006; Cody & Schwalbe, 2006), the side chain of the conserved Arg75 in pcDHFR is held in place by a network of hydrogen bonds to the conserved Thr40 and Ser41 and the backbone functional groups of Lys73 (Fig. 4). These conserved contacts are independent of ligand binding. There is also a *cis*-peptide linkage between Arg67 and Pro68 and between Gly124 and Gly125, as observed in other pcDHFR complexes. The interactions of the 2,4-diaminopyrido[2,3-*d*]pyrimidine ring of this antifolate preserve the overall pattern of contacts with invariant residues in the active site. The hydrogen-bond network involving structural

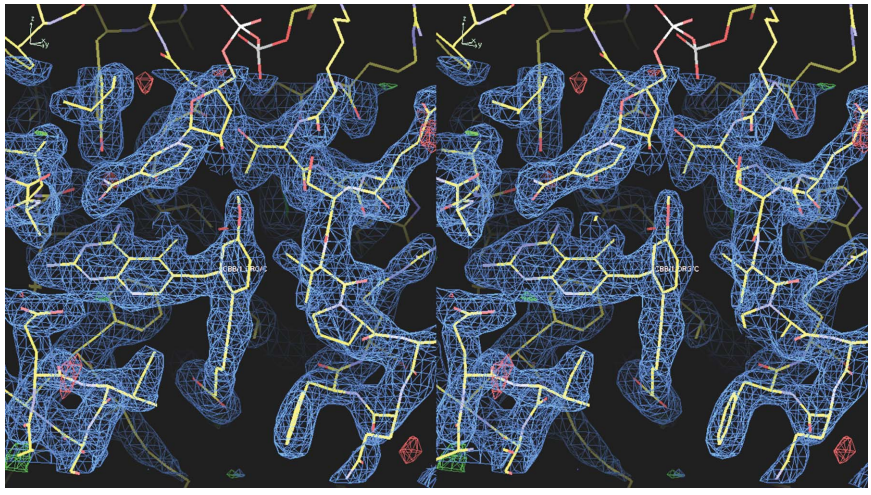

Figure 2
Stereoview of the pcDHFR–NADPH–PY1014 electron-density map ($2F_o - F_c$, 0.9σ).

water, the conserved residues Thr144, Trp27 and Glu32, and the N1 nitrogen and 2-amino group of the pyrido[2,3-*d*]pyrimidine ring are also maintained. Similarly, the inhibitor 4-amino group maintains its contacts with the conserved residues Ile9 and Tyr129 and NADPH (Cody & Schwalbe, 2006).

The 2′-carboxypentynyloxybenzyl side chain of PY1014 is similar to that of the previously reported potent 5′-carboxy-1-pentynyloxybenzyl pyrimidine analog PY1011 (Rosowsky *et al.*, 2004; Cody *et al.*, 2006; Fig. 1). There is a correlation between changes in the torsion angles that describe the bridging geometry between the ring systems (C5–C6–C7–C1′/C6–C7–C1′–C2′) of PY1014 (Fig. 1, Table 1) and the orientation of the side chain. The structural results show that despite the difference in the size of the pyrimidine ring of the TMP template compared with the pyrido[2,3-*d*]pyrimidine ring, the 2′-carboxypentynyloxybenzyl side chain of PY1014 adjusts its conformation to form a salt bridge with Arg75 (Cody *et al.*, 2006; Cody & Pace, 2011; Fig. 5). Additionally, the pyrido[2,3-*d*]pyrimidine ring of PY1014 places the 5′-methoxy group closer to Leu25 and Ser64 than is observed for the interaction of the 3′,4′-dimethoxy groups of PY1011 (Cody *et al.*, 2006; Fig. 5). The 5′-methoxy O atom of PY1014 forms a hydrogen bond to the amide of Leu25 (O···N, 2.7 Å) and the methoxy methyl group makes a hydrophobic contact of 3.1 Å with C^{β} of Ser64. These contacts are 4.2 and 3.3 Å, respectively, for the 3′-methoxy group in the PY1011 complex. Comparison of the structures of the pyrido[2,3-*d*]pyrimidines PY1014 and PY996 reveals that adjustments in the bridging torsion angles permit the interaction of the carboxylate side chain with Arg75 to be conserved despite the side-chain conformational differences (Fig. 5). The full conformational range of these analogs is illustrated in Fig. 6.

4. Discussion

The results of the structural study of the *O*-(*ω*-carboxypentynyl) analog PY1014 (Fig. 1) revealed that the carboxypentynyl side chain makes optimal interactions with the conserved Arg75 in the active site of pcDHFR, as observed for the pyrimidine carboxylalkynyl analog PY1011, despite the increased size of the pyrido[2,3-*d*]-pyrimidine ring. Comparison of these structures shows that there is a change in the bridging conformation that permits the side chain to optimize its interactions with Arg75. The interactions of the side chain of PY1014 with Arg75 are also similar to those of the pyrido[2,3-*d*]pyrimidine PY996 (Fig. 6).

Structure–activity correlations for the 2,4-diaminopyrimidine analogs PY1011 and PY957 reveal that the combined effect of the 3′,4′-dimethoxy substituents and the 5′-pentynyl carboxy side chain of PY1011 *versus* the 2′-methoxy-5′-carboxy-1-butynyloxy side chain of PY957 contributes to the extraordinary selectivity of PY1011 for

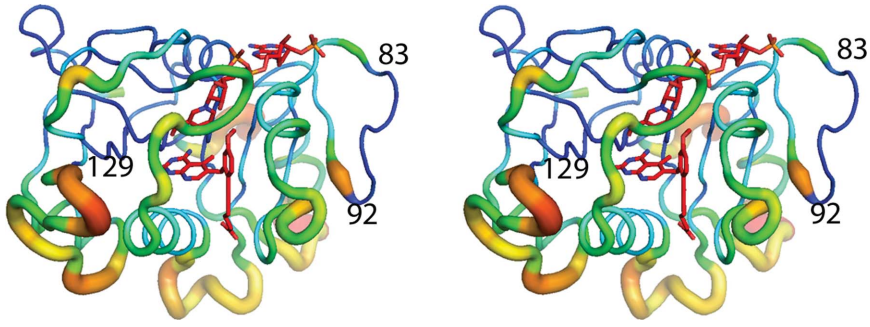

Figure 3
Stereoview of the pcDHFR ternary complex with PY1014 and NADPH (red stick figures) showing the thermal parameters using the '*B*-factor Putty' function in *PyMOL*. The regions shown in red/orange have the highest *B* values (residues 1–4 and 83–92 were not used in the refinement) and those in yellow ranged from 50 to 60 Å^2, compared with values of 20–40 Å^2 for the more stable green and blue regions. The residues in loop 83–92 were not refined and their *B* values were set to a fixed value for this plot.

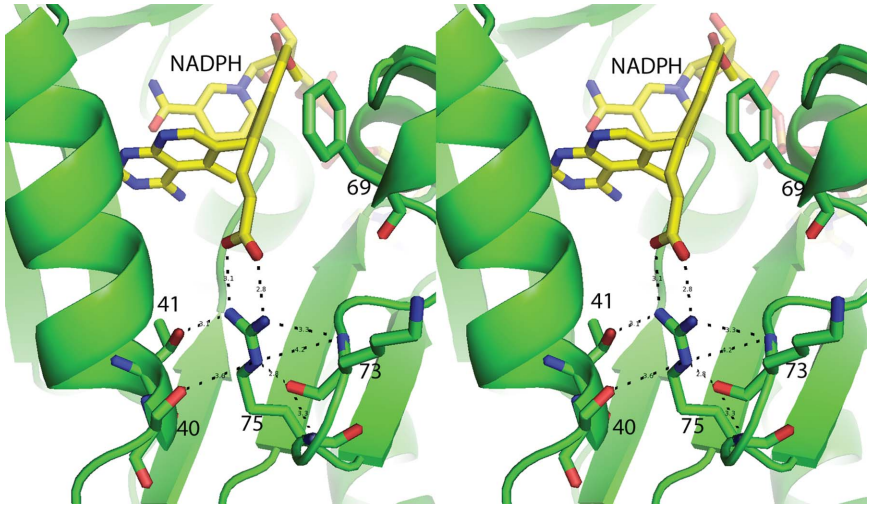

Figure 4
Conserved intermolecular contacts involving Arg75 of pcDHFR (green) and the inhibitor PY1011 (yellow) showing interactions with Thr41 (O···NH_2, 3.1 Å), Ser40 (O···NH, 3.6 Å), the backbone carbonyl of Lys73 (O···NH, 2.8 Å), Lys73 (O···NH, Arg75 3.3 Å), Lys73 (N···NH, 4.2 Å) and the carboxylate of PY1011 (O1···NH_2, 3.1 Å; O2···NH_2, 2.8 Å). Residue Phe69 and NADPH are also labeled.

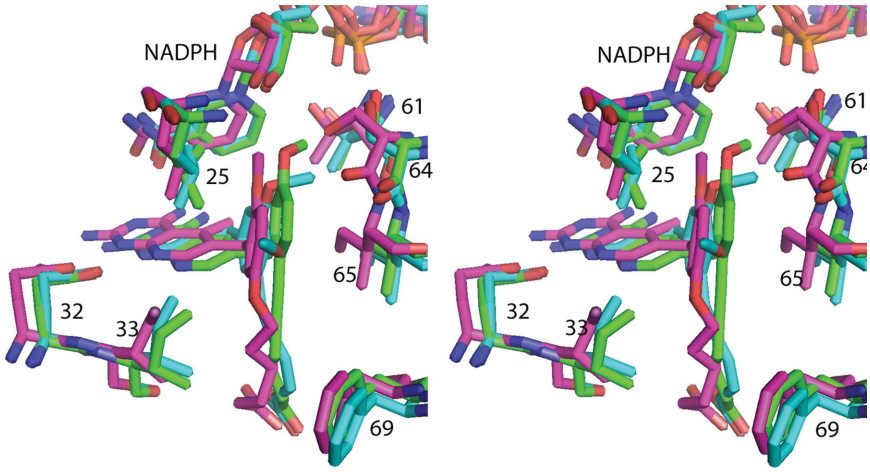

Figure 5
Stereo superposition of PY1014 (green) with PY1011 (cyan; Cody *et al.*, 2006) and PY996 (violet; Cody & Pace, 2011) in the structures of their ternary complexes with pcDHFR and NADPH. The active-site residues Leu25, Glu32, Ile33, Thr61, Ser64, Leu65 and Phe69 are shown.

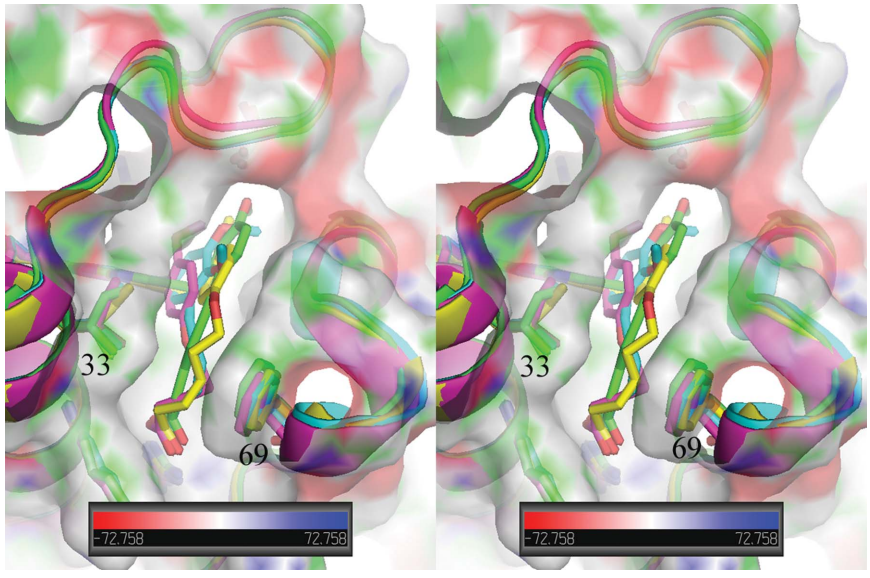

Figure 6
Stereoview showing the electrostatic surface of pcDHFR in ternary complexes with NADPH and the inhibitors PY1014 (green), PY1011 (cyan), PY957 (yellow) and PY996 (violet). Also shown are the active-site residues Ile33 and Phe69 that make hydrophobic contacts with the methylene C atoms of the side chains of the analogs.

pcDHFR (5000-fold *versus* 80-fold selectivity for pcDHFR). However, similar substitutions in the 2,4-diaminopyrido[2,3-*d*]pyrimidines revealed uniformly weaker selectivity for the series. Although the binding of PY1014 and PY1011 appear to be similar in their respective crystal structures (Fig. 5), the substitution pattern in PY1014 differs from that of PY1011, *i.e.* a 2′-pentynylcarboxy-5′-methoxy substitution pattern in PY957 *versus* a 2′-methoxy-5′-carbobutyloxy substitution pattern in PY996. Even though the IC_{50} values of PY1014, PY1011 and PY996 are similar, inhibition data show that the selectivity of PY1011 is significantly greater for pcDHFR than PY1014, PY957 and PY996, which has a longer side chain [$(CH_2)_5$ *versus* $(CH_2)_3$]. The greater pcDHFR selectivity of PY1014 compared with mammalian DHFR also results from enhanced hydrophobic interactions of the methylene groups with Phe69 compared with Asn64 in the mammalian DHFR. The 5′-methoxyl group of PY1014 probes deeper into the active-site pocket than the 2′-methoxy group of PY996 (Fig. 6). The ability of these inhibitors to probe different portions of the active-site pocket is correlated with differences in their potency and selectivity.

In summary, these results help to explain the weaker potency and selectivity of the pyrido[2,3-*d*]pyrimidine *O*-[*ω*-carboxyalkynylbenzyl] scaffold in this series of DHFR inhibitors compared with homologous analogs in the pyrimidine series (Chan *et al.*, 2005; Rosowsky *et al.*, 2004).

This work was supported in part by a grant from the National Institutes of Health GM51670 (VC). The authors thank Dr Andre Rosowsky for supplying the antifolates and the beamline staff at SSRL for their support. Portions of this research were carried out at the Stanford Synchrotron Radiation Laboratory, a national user facility operated by Stanford University on behalf of the US Department of Energy, Office of Basic Energy Sciences. The SSRL Structural Molecular Biology Program is supported by the Depart-

ment of Energy, Office of Biological and Environmental Research and by the National Institutes of Health, National Center for Research Resources, Biomedical Technology Program and the National Institute of General Medical Sciences.

References

Chan, D. C. M., Fu, H., Forsch, R. A., Queener, S. F. & Rosowsky, A. (2005). *J. Med. Chem.* **48**, 4420–4431.
Cody, V., Galitsky, N., Rak, D., Luft, J. R., Pangborn, W. & Queener, S. F. (1999). *Biochemistry*, **38**, 4303–4312.
Cody, V., Luft, J. R. & Pangborn, W. (2005). *Acta Cryst.* D**61**, 147–155.
Cody, V. & Pace, J. (2011). *Acta Cryst.* D**67**, 1–7.
Cody, V., Pace, J., Chisum, K. & Rosowsky, A. (2006). *Proteins*, **65**, 959–969.
Cody, V., Pace, J., Makin, J., Piraino, J., Queener, S. F. & Rosowsky, A. (2009). *Biochemistry*, **48**, 1702–1711.
Cody, V. & Schwalbe, C. H. (2006). *Crystallogr. Rev.* **12**, 301–333.
Cohen, A. E., Ellis, P. J., Miller, M. D., Deacon, A. M. & Phizackerley, R. P. (2002). *J. Appl. Cryst.* **35**, 720–726.
DeLano, W. L. (2002). *PyMOL*. http://www.pymol.org.
Emsley, P., Lohkamp, B., Scott, W. G. & Cowtan, K. (2010). *Acta Cryst.* D**66**, 486–501.
Evans, P. (2006). *Acta Cryst.* D**62**, 72–82.
Forsch, R. A., Queener, S. F. & Rosowsky, A. (2004). *Bioorg. Med. Chem. Lett.* **14**, 1811–1815.
González, A., Moorhead, P., McPhillips, S. E., Song, J., Sharp, K., Taylor, J. R., Adams, P. D., Sauter, N. K. & Soltis, S. M. (2008). *J. Appl. Cryst.* **41**, 176–184.
Krissinel, E. & Henrick, K. (2004). *Acta Cryst.* D**60**, 2256–2268.
Lovell, S. C., Davis, I. W., Arendell, W. B. III, de Baker, P. I. W., Word, J. M., Prisant, M. G., Richardson, J. S. & Richardson, D. C. (2002). *Proteins*, **50**, 437–450.
McPhillips, T. M., McPhillips, S. E., Chiu, H.-J., Cohen, A. E., Deacon, A. M., Ellis, P. J., Garman, E., Gonzalez, A., Sauter, N. K., Phizackerley, R. P., Soltis, S. M. & Kuhn, P. (2002). *J. Synchrotron Rad.* **9**, 401–406.
Murshudov, G. N., Skubák, P., Lebedev, A. A., Pannu, N. S., Steiner, R. A., Nicholls, R. A., Winn, M. D., Long, F. & Vagin, A. A. (2011). *Acta Cryst.* D**67**, 355–367.
Nahimana, A., Rabodonirina, M., Bille, J., Francioli, P. & Hauser, P. M. (2004). *Antimicrob. Agents Chemother.* **48**, 4301–4305.
Otwinowski, Z. & Minor, W. (1997). *Methods Enzymol.* **276**, 307–326.
Rosowsky, A., Forsch, R. A. & Queener, S. F. (2003). *J. Med. Chem.* **46**, 1726–1736.
Rosowsky, A., Fu, H., Chan, D. C. M. & Queener, S. F. (2004). *J. Med. Chem.* **47**, 2475–2485.
Schüttelkopf, A. W. & van Aalten, D. M. F. (2004). *Acta Cryst.* D**60**, 1355–1363.
Thomas, C. F. & Limper, A. H. (2004). *N. Engl. J. Med.* **350**, 487–2498.
Vagin, A. & Teplyakov, A. (2010). *Acta Cryst.* D**66**, 22–25.
Winn, M. D. *et al.* (2011). *Acta Cryst.* D**67**, 235–242.